

Influence of matching field on critical current density and irreversibility temperature in $\text{YBa}_2\text{Cu}_3\text{O}_7$ films with BaMO_3 (M = Zr, Sn, Hf) nanorods

Cite as: Appl. Phys. Lett. **108**, 082601 (2016); <https://doi.org/10.1063/1.4942463>

Submitted: 20 December 2015 . Accepted: 09 February 2016 . Published Online: 24 February 2016

Tomoya Horide, Kenta Taguchi, Kaname Matsumoto, Naoki Matsukida, Manabu Ishimaru, Paolo Mele, and Ryusuke Kita



View Online



Export Citation



CrossMark

ARTICLES YOU MAY BE INTERESTED IN

Improvement in J_c performance below liquid nitrogen temperature for $\text{SmBa}_2\text{Cu}_3\text{O}_y$ superconducting films with BaHfO_3 nano-rods controlled by low-temperature growth

APL Materials **4**, 016102 (2016); <https://doi.org/10.1063/1.4939182>

Pin potential effect on vortex pinning in $\text{YBa}_2\text{Cu}_3\text{O}_{7-\delta}$ films containing nanorods: Pin size effect and mixed pinning

Applied Physics Letters **110**, 052601 (2017); <https://doi.org/10.1063/1.4975300>

Strongly enhanced vortex pinning from 4 to 77 K in magnetic fields up to 31 T in 15 mol.% Zr-added (Gd, Y)-Ba-Cu-O superconducting tapes

APL Materials **2**, 046111 (2014); <https://doi.org/10.1063/1.4872060>

Applied Physics Reviews
Now accepting original research

2017 Journal
Impact Factor:
12.894

Influence of matching field on critical current density and irreversibility temperature in $\text{YBa}_2\text{Cu}_3\text{O}_7$ films with BaMO_3 ($M = \text{Zr, Sn, Hf}$) nanorods

Tomoya Horide,^{1,a)} Kenta Taguchi,¹ Kaname Matsumoto,¹ Naoki Matsukida,¹ Manabu Ishimaru,¹ Paolo Mele,² and Ryusuke Kita³

¹Department of Materials Science and Engineering, Kyushu Institute of Technology, 1-1 Sensui-cho, Tobata-ku, Kitakyushu 804-8550, Japan

²College of Design and Manufacturing Technology, Muroran Institute of Technology, 27-1 Mizumoto-cho, Muroran, Hokkaido 050-8585, Japan

³Graduate School of Integrated Science and Technology, Shizuoka University, 3-5-1 Johoku, Naka-ku, Hamamatsu 432-8561, Japan

(Received 20 December 2015; accepted 9 February 2016; published online 24 February 2016)

The influence of the matching field (B_Φ) on critical current density (J_c) and irreversibility temperature (T_{irr}) in $\text{YBa}_2\text{Cu}_3\text{O}_7$ films containing BaMO_3 ($M = \text{Zr, Sn, Hf}$) nanorods was investigated. It was revealed that the irreversibility temperature normalized by the critical temperature (T_{irr}/T_c) was influenced by B_Φ , for $B > B_\Phi$, but T_{irr}/T_c did not depend on which BaMO_3 material was used for $B < B_\Phi$, i.e., there was no dependence on nanorod density, diameter, interface sharpness, or T_c in the case of ideal nanorods. However, $J_c/J_c(0\text{ T})$ was found to decrease with increasing B_Φ at low magnetic field strengths and to improve at high magnetic field strengths. In addition to J_c being dependent on B_Φ , the T_c term in T_{irr} and $J_c(0\text{ T})$ were also found to have an effect on J_c . © 2016 AIP Publishing LLC.

[<http://dx.doi.org/10.1063/1.4942463>]

Artificial pinning centers (APCs) significantly improve critical current density (J_c) in $\text{YBa}_2\text{Cu}_3\text{O}_7$ (YBCO) films. BaMO_3 (BMO; $M = \text{Zr, Sn, Hf}$) nanorods are one of the most effective APCs for obtaining a high J_c and global pinning force maximum ($F_{p,\text{max}}$).^{1–3} A very high J_c was achieved with a high nanorod density at a high magnetic field and low temperature,⁴ while shape control of the nanorods and hybrid APCs resulted in systematic variation of the vortex pinning.^{5–8} These results show that BMO nanorods are promising for controlling the vortex pinning and enhancing J_c . Elastic strain,⁹ oxygen vacancies,¹⁰ and defect-induced strain fields¹¹ change the matrix critical temperature (T_c) and elementary pinning force (f_p) in YBCO + BMO films. Geometric factors of the nanorods are also crucial to vortex pinning and dynamics: the straightness of the nanorods and their size determine the pinned volume, while the matching field (B_Φ) is proportional to their density. Although B_Φ is believed to be one of the most important factors and many researchers observed B_Φ -induced phenomena in YBCO that contained c -axis correlated pinning centers,^{6,12–16} there is a lack of systematic studies on this topic, and therefore, the influence of B_Φ on J_c remains unclear. To further understand the c -axis correlated pinning induced by BMO nanorods, a detailed analysis of vortex pinning is needed for YBCO + BMO films whose B_Φ is systematically varied.

The dependence of J_c on BMO content was extensively studied to optimize J_c in YBCO + BMO films.^{17,18} Because the microstructure depends on BMO content, YBCO + BMO films with varying BMO content are a well-defined system with which to study c -axis correlated pinning induced by BMO nanorods. However, no previous research has studied the dependence of J_c on BMO content to understand vortex behavior. In this study, therefore, B_Φ was systematically

controlled by varying BMO content and the M in BMO, while measuring J_c as a function of B_Φ . Based on the results, the influence of B_Φ , $J_c(0\text{ T})$, and T_c on J_c is discussed to understand the mechanisms that determine J_c in YBCO + BMO films.

YBCO films were prepared on SrTiO_3 (100) single crystalline substrates at 830 °C and 0.26 mbar using pulsed laser deposition (PLD). YBCO + BZO, YBCO + BSO, and YBCO + BaHfO_3 (BHO) mixed targets were ablated, where BSO, BZO, and BHO content of the targets were 2.7–7.2 vol. %, 4.1–8.2 vol. %, and 3.1–6.3 vol. %, respectively; the films fabricated in this manner are referred to as YBCO + BZO(X), YBCO + BSO(X), and YBCO + BHO(X) in this letter, where X is the vol. % of BZO, BSO, or BHO. The resulting film thicknesses were 150–240 nm. The microstructure of the films was observed using transmission electron microscopy (TEM). Then, 1-mm long and 100- μm wide bridges were formed using conventional photolithography and H_3PO_4 etching to measure J_c with Physical Property Measurement System (PPMS). The magnetic field dependence of J_c was evaluated at 65–77 K under a magnetic field of 0–9 T, while the temperature (T) dependence of the resistivity was measured to obtain the irreversibility temperature (T_{irr}). J_c and T_{irr} measurements were performed mainly under a magnetic field parallel to the c -axis; J_c and T_{irr} were determined at an electric field strength of 1 $\mu\text{V}/\text{cm}$. Table I summarizes basic parameters in the films.

Figure 1 shows cross-sectional bright-field TEM images of YBCO + BZO(4.1), YBCO + BSO(2.7), and YBCO + BHO(4.7) films. It is apparent from these images that BMO nanorods grow in the c -axis direction of YBCO, and ideal c -axis correlated pinning is, therefore, expected in these films. Nanorod diameter (D) was 6 nm, 10 nm, and 6 nm, and the spacing of nanorods (d) was ~ 20 nm, 25–33 nm, and ~ 20 nm in the YBCO + BZO(4.1), YBCO + BSO(2.7), and YBCO + BHO(4.7) films, respectively.

^{a)}Author to whom correspondence should be addressed. Electronic mail: horide@post.matsc.kyutech.ac.jp

TABLE I. Summary of basic parameters in the films.

Material	BMO content (vol. %)	Thickness (nm)	T_c (K)	J_c at 77 K, 0 T (MA/cm ²)	$F_{p,max}$ at 77 K (GN/m ³)	$F_{p,max}$ at 65 K (GN/m ³)
BSO	2.7	210	89.2	2.4	14.6	47.7
BSO	5.4	210	87.8	...	12.4	45.5
BSO	7.2	150	86.9	1.0	3.0	11.4
BZO	4.1	190	88.2	1.6	15.8	66.8
BZO	8.2	160	87.1	1.8	17.0	85.4
BHO	3.1	190	88.9	0.65	3.8	...
BHO	4.7	160	87.5	0.95	8.1	60.4
BHO	6.3	180	85.9	0.82	6.9	50.8

Figure 2 shows the magnetic field dependence of T_{irr} in (a) the YBCO + BZO, (b) YBCO + BSO, and (c) YBCO + BHO films. For comparison, T_{irr} normalized by T_c (T_{irr}/T_c) is also shown in Fig. 2(d). $B-T_{irr}$ curves exhibit a shoulder at 1–5 T, and it is well known that the shoulder appears at

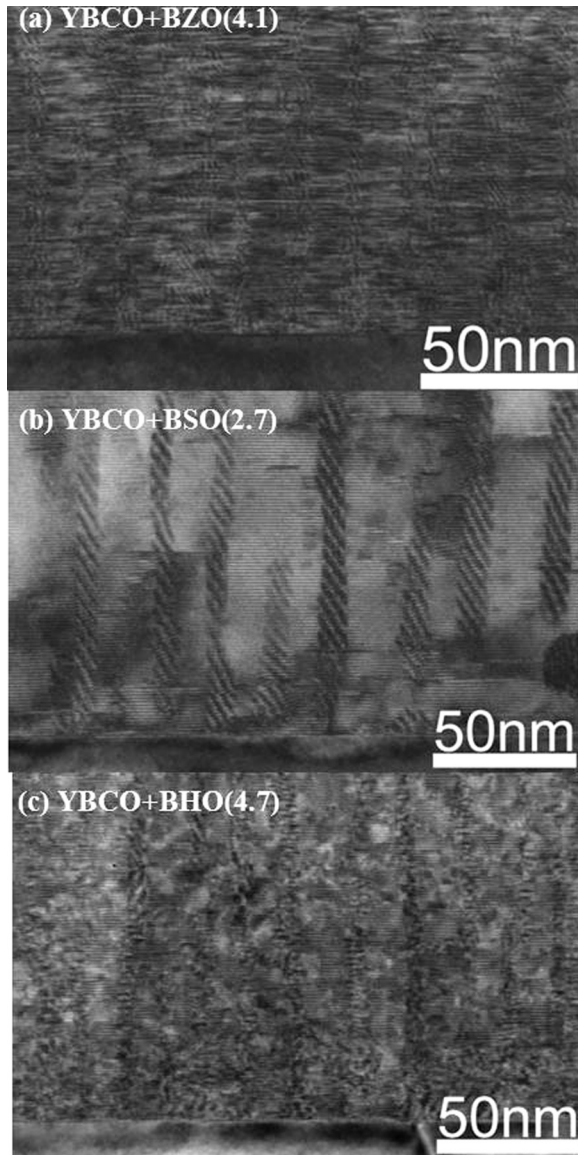


FIG. 1. Cross-sectional bright-field TEM images of (a) YBCO + BZO(4.1), (b) YBCO + BSO(2.7), and (c) YBCO + BHO(4.7) films. BMO nanorods grew in the c -axis direction of YBCO. d was ~ 20 nm, 25–33 nm, and ~ 20 nm in the YBCO + BZO(4.1), YBCO + BSO(2.7), and YBCO + BHO(4.7) films, respectively.

B_Φ .^{13–16} T_{irr}/T_c behavior was in good agreement in the $B < B_\Phi$ range, regardless of nanorod structure, but it depended on nanorod structure in the $B > B_\Phi$ range. From the shoulder that corresponds to the crossover between structure-independent T_{irr}/T_c and structure-dependent T_{irr}/T_c , B_Φ was estimated to be 3.75 ± 0.5 T for YBCO + BZO(4.1), 1.5 ± 0.5 T for YBCO + BSO(2.7), and 4.5 ± 0.5 T for YBCO + BHO(4.7). Because B_Φ is given by $n\phi_0$ (n : nanorod density, ϕ_0 : magnetic flux quantum = 2.07×10^{-15} Wb), we used the TEM results to calculate B_Φ as ~ 5 T for YBCO + BZO(4.1), ~ 2.5 T for YBCO + BSO(2.7), and ~ 5 T for YBCO + BHO(4.7). B_Φ values obtained from the T_{irr} and TEM measurements were thus in good agreement. Figure 2(e) shows the dependence of B_Φ on BMO content that was estimated from the $B-T_{irr}$ curves; B_Φ and BMO volume fraction are given by ϕ_0/d^2 and $\pi D^2/4d^2$, respectively. The results show that for small or moderate BMO content B_Φ increased with increasing BMO content. However, B_Φ decreased in the YBCO + BSO(7.2) and YBCO + BZO(8.2) samples, which have high BMO content, suggesting that an increase in nanorod diameter was to blame, especially because it has been previously reported that too high BMO content may result in degradation of the nanorod structure.¹⁸ These results suggest that ideal c -axis correlated pinning was not achieved when the BMO content was too high, and therefore, we exclude the results in which BMO content was too high from our discussion of ideal nanorod pinning.

Figure 2(f) shows T_{irr}/T_c at 1 T and 7 T as a function of B_Φ for ideal c -axis correlated pinning. T_{irr}/T_c did not depend on BMO content at 1 T ($< B_\Phi$) owing to the strong Bose glass.¹⁹ T_{irr}/T_c increased with increasing B_Φ at 7 T ($> B_\Phi$), indicating that T_{irr} behavior in the $B > B_\Phi$ range was determined only by B_Φ , not by BMO selection. A similar tendency was also observed for $\text{SmBa}_2\text{Cu}_3\text{O}_7 + \text{BHO}$,²⁰ $\text{SmBa}_2\text{Cu}_3\text{O}_7 + \text{BSO}$,²⁰ and $\text{GdBa}_2\text{Cu}_3\text{O}_7 + \text{BHO}$ ²¹ even if Y in YBCO was changed to other rare earth elements.

Figure 3(a) shows J_c-B curves at 77 K for YBCO + BZO(4.1), YBCO + BSO(2.7), YBCO + BHO(4.7), and pure YBCO films. BMO incorporation improved J_c , especially at high magnetic field strengths. Figure 3(b) shows the temperature and field angle dependence of the J_c-B curve for the YBCO + BSO(2.7) film. The magnetic field was applied along the ab plane ($B//ab$) and along the c -axis ($B//c$). Clear shoulders were observed in the J_c-B curves only for $B//c$; additionally, J_c was much higher for $B//c$ than for $B//ab$ at 1–3 T. In contrast, the pure YBCO films do not exhibit such strong c -axis correlated pinning.²² Figures 3(c)–3(f) show J_c

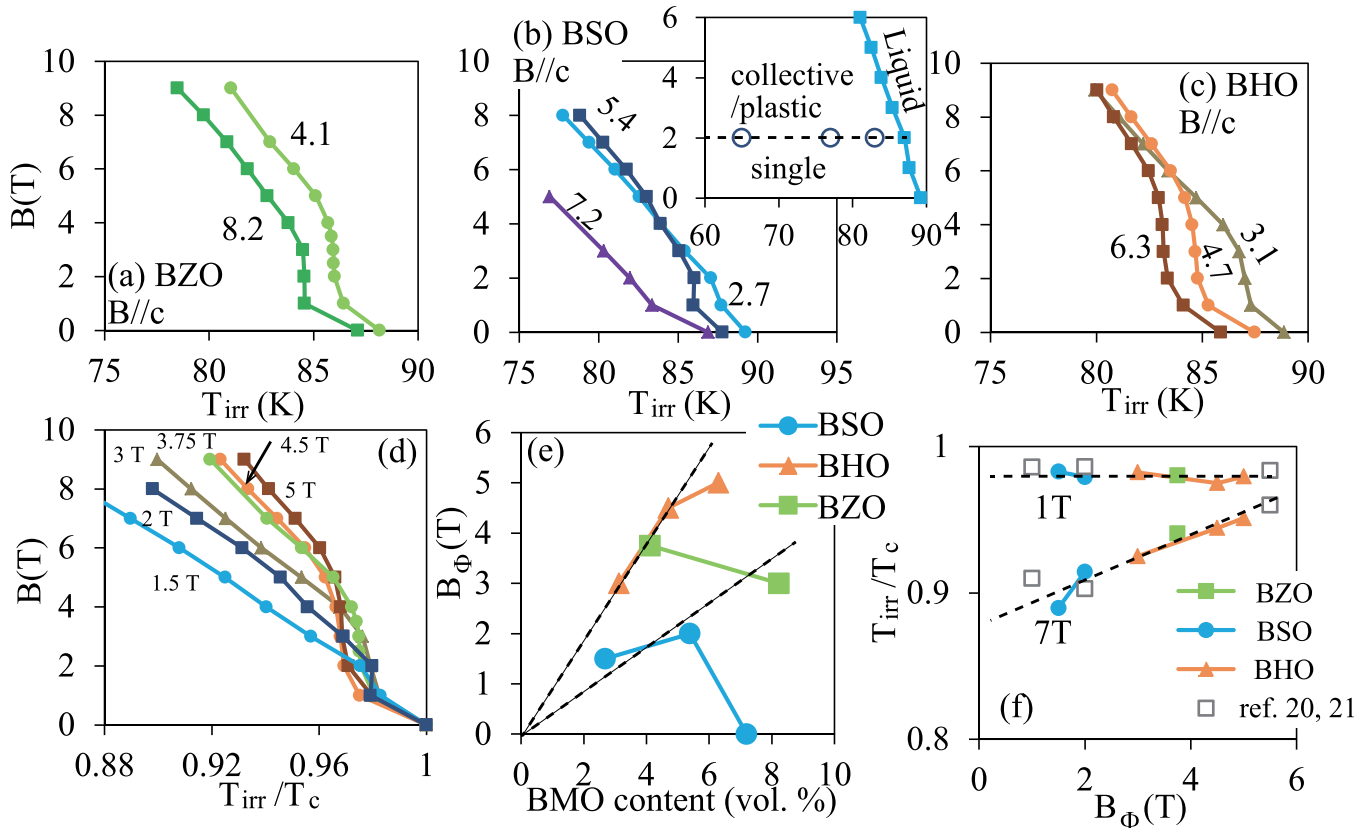


FIG. 2. B - T_{irr} curves in (a) YBCO+BZO, (b) YBCO+BSO, and (c) YBCO+BHO films. Inset of (b) shows vortex phase diagram in the YBCO+BSO(2.7) sample, where the field of shoulder in J_c - B and T_{irr} (\sim the Bose glass temperature) defines the regions for single vortex pinning (the strong Bose glass), collective/plastic vortex pinning (the weak Bose glass), and vortex liquid. (d) B - T_{irr}/T_c curves as a function of B_Φ for the YBCO+BMO films with ideal nanorod pinning. The same symbols as used in (a)–(c) are used in (d). (e) Dependence of B_Φ on BMO vol. % content. The lines show the B_Φ -BMO content relationship with constant nanorod diameter. (f) Dependence of T_{irr}/T_c on B_Φ at 1 T and 7 T. The results from Refs. 20 and 21 are also plotted. All data were obtained with $B//c$.

as a function of BMO content at various temperatures and magnetic field values. YBCO+BSO(2.7) exhibited the highest J_c at a low magnetic field of 1 T, while increasing BSO concentration to 7.2 vol. % did not improve J_c , regardless of applied magnetic field and temperature. BZO and BHO incorporation did not increase J_c in the low magnetic field range of 0–1 T but significantly improved J_c at higher magnetic field strengths. J_c was higher in YBCO+BZO than in YBCO+BHO, regardless of temperature and applied magnetic field, and large J_c was achieved at high magnetic fields at both 4.1 vol. % and 8.2 vol. % BZO content. It is difficult to achieve a high density of BSO nanorods because of their large diameter; however, because of their smaller diameters, the density of BZO and BHO nanorods can be increased. The present results are consistent with previous reports: heavy Zr doping into (Gd,Y)BCO significantly improved J_c at a low temperature and a high magnetic field,²³ while high J_c in films with a high BSO content has not yet been reported.¹⁷

Similar to the influence of B_Φ on T_{irr}/T_c , B_Φ is expected to have a significant effect on J_c . To illustrate the influence of B_Φ on J_c , Fig. 4(a) shows $J_c/J_c(0\text{T})$ at 77 K for the YBCO+BMO films. The highest $J_c/J_c(0\text{T})$ values in the 0.5–2 T and 7–9 T range were obtained for the YBCO+BSO(2.7) and YBCO+BHO(6.3) films, respectively. Conversely, the lowest $J_c/J_c(0\text{T})$ values in the 0.5–2 T and 7–9 T range were obtained for the YBCO+BHO(6.3) and YBCO+BSO(2.7)

films, respectively. The YBCO+BSO(2.7) and YBCO+BHO(6.3) films had the lowest and the highest B_Φ in this study, respectively. With increasing B_Φ , $J_c/J_c(0\text{T})$ decreased at low magnetic field strengths but increased at high magnetic field strengths, demonstrating a systematic variation of the J_c - B curves with B_Φ . Behavior of J_c similar to that observed at 77 K was also observed at 65 K (shown in Fig. 4(b)). $F_p/F_{p\text{max}}$ - B curves at 77 K and 65 K are shown in Figs. 4(c) and 4(d), where $F_{p\text{max}}$ was obtained at the peak magnetic field (B_p). B_p was 2 T and 6 T in the YBCO+BSO(2.7) and YBCO+BHO(6.3) films, respectively, and B_p increased from 2 T to 6 T with increasing B_Φ at 77 K. B_p ranged from 3 T for YBCO+BSO(2.7) to 8 T for YBCO+BHO(6.3) at 65 K, depending on B_Φ . The vortex phase diagram of the YBCO+BSO(2.7) sample is shown in Fig. 2(b). Strong nanorod pinning and a temperature-independent shoulder-field ($\sim B_p$) indicate that the shoulder in the J_c - B curve did not result from the transition from Bragg glass to vortex glass,²⁴ but from the B_Φ effect. Vortices are pinned by nanorods for $B < B_\Phi$ and by elastic interactions for $B > B_\Phi$. J_c for $B < B_\Phi$ is constant in the single vortex pinning region without thermal fluctuation, which is achieved at a low temperature.^{15,25,26} As shown in Fig. 4, in the single vortex pinning region, J_c gradually decreases with the magnetic field because of thermal fluctuations at high temperatures such as 65–77 K.^{14,26} $J_c/J_c(0\text{T})$ values for the YBCO+BSO(2.7) sample were 0.75, 0.41, and

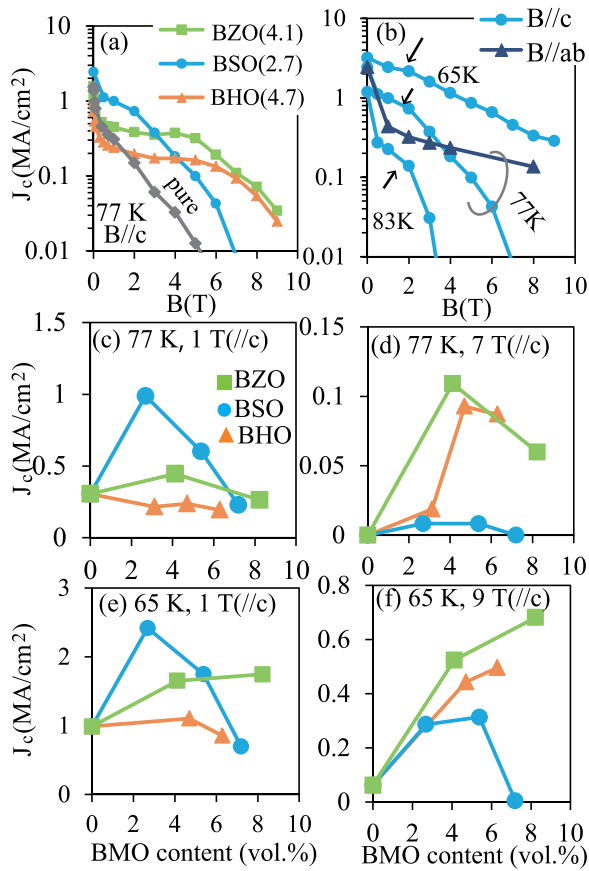


FIG. 3. (a) J_c - B curves with $B//c$ at 77 K in the YBCO + BZO(4.1), YBCO + BSO(2.7), and YBCO + BHO(4.7) films. (b) Temperature and field angle dependence of J_c - B curves for the YBCO + BSO(2.7) films. Magnetic field was applied for $B//ab$ and $B//c$ at 77 K. Clear shoulders in the J_c - B curves (indicated by arrows) were observed only for $B//c$. J_c as a function of BMO content at (c) 77 K, 1 T, (d) 77 K, 7 T, (e) 65 K, 1 T, and (f) 65 K, 9 T. The same symbols are used in (c)-(f). YBCO + BSO(2.7) exhibited the highest J_c at low magnetic field strengths, while the highest J_c at high magnetic field strengths was achieved with 4.1 vol. % and 8.2 vol. % BZO content.

0.19 at 65 K, 77 K, and 83 K under a magnetic field of 1 T, while $J_c/J_c(0 T)$ values were 0.35 and 0.18 at 65 K and 77 K under a magnetic field of 3 T for the YBCO + BSO(4.7) film. $J_c/J_c(0 T)$ decreased with increasing temperature, indicating a thermal fluctuation effect on J_c in the single vortex pinning region ($B < B_\Phi$) at high temperatures. The motion of thermally fluctuating vortices is accelerated by neighboring unoccupied nanorods for $B < B_\Phi$, and the acceleration becomes significant when nanorod spacing is small. As neighboring nanorods are occupied by vortices at $\sim B_\Phi$, thermally assisted vortex motion to unoccupied nanorods becomes difficult. Thus, J_c rapidly decreases with increasing magnetic field strengths around $\sim 0 T$ for small nanorod spacings, i.e., for large B_Φ . Because the elastic interaction of vortices is weaker than direct pinning of nanorods, and high-density nanorods can accommodate many vortices, J_c was improved through a high density of nanorods at high magnetic field strengths.

Figures 5(a)-5(d) show J_c as a function of B_Φ at 77 K and 65 K under magnetic fields of 1 T, and 7 T and 9 T, respectively, where B_Φ was obtained from T_{irr} . Although large J_c was obtained at low magnetic field strengths of 1 T for the films with small B_Φ , large B_Φ enhanced J_c at high magnetic field strengths of 7 T and 9 T. However, B_Φ accounted only, in

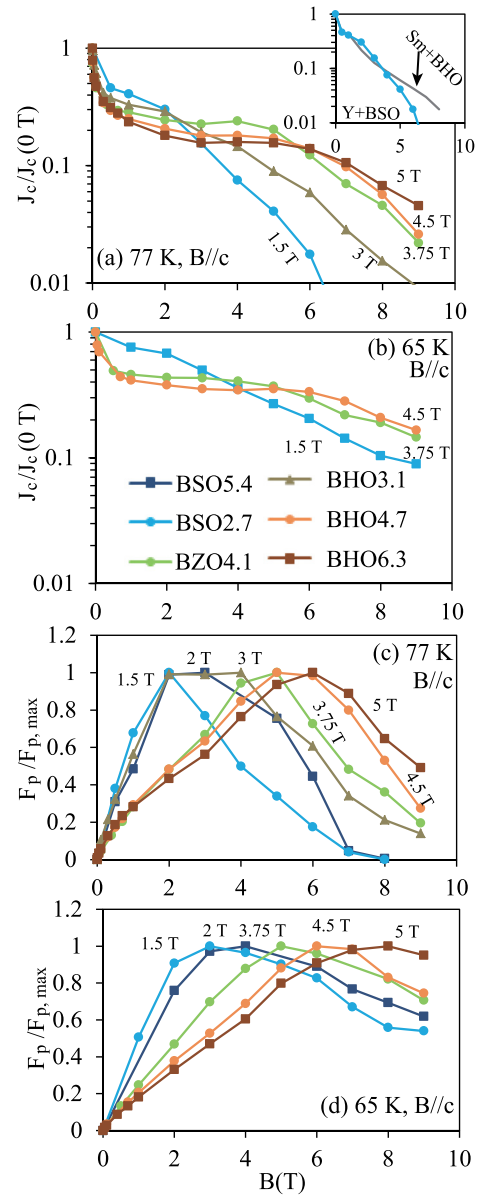


FIG. 4. $J_c/J_c(0 T)$ - B curves for the films for $B//c$ at (a) 77 K and (b) 65 K. Inset of (a) compares $J_c/J_c(0 T)$ - B curve of the YBCO + BSO(2.7) film with that of the SmBa₂Cu₃O₇ + BHO sample reported in Fig. 5 of Ref. 20. $F_p/F_{p,max}$ - B curves for the films at (c) 77 K and (d) 65 K. The same symbols and B_Φ values are used in (a)-(d). $J_c/J_c(0 T)$ - B curves and $F_p/F_{p,max}$ - B curves systematically vary with B_Φ .

part, for the magnetic field dependence of J_c that is visible in Fig. 5, because a single function of B_Φ cannot describe J_c , demonstrating that other factors also affect J_c .

Although $J_c(0 T)$ may depend on B_Φ , its effect on J_c is worth discussing separately to understand the mechanisms that influence J_c . The effect of $J_c(0 T)$ is discussed for the YBCO + BHO(4.7) and YBCO + BZO(4.1) films, where J_c was different despite having almost the same B_Φ of ~ 4 -5 T. $J_c(0 T)$ is dependent on the current flow path, film homogeneity, f_p , matrix crystallinity, and T_c . $J_c(\text{YBCO + BZO}(4.1))/J_c(\text{YBCO + BHO}(4.7))$ at 3 T was 2.1 and 1.6 at 77 K and 65 K. The J_c ratio depended on temperature, suggesting that f_p , matrix crystallinity, and T_c were the dominant factors causing the difference in $J_c(0 T)$ between the YBCO + BHO(4.7) and YBCO + BZO(4.1) samples.

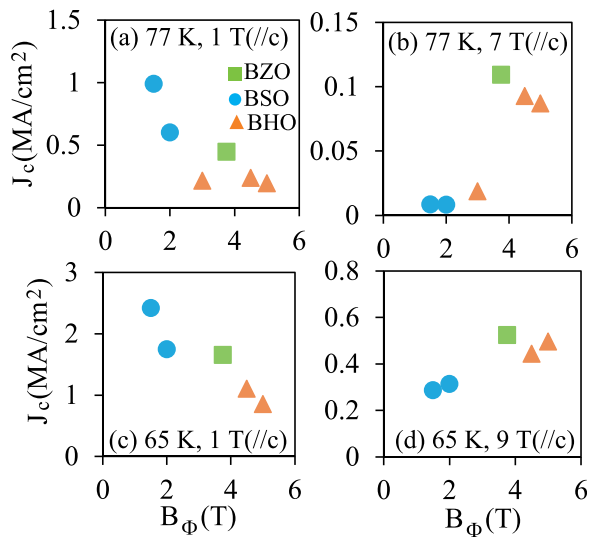


FIG. 5. B_{Φ} dependence of J_c at (a) 77 K, 1 T, (b) 77 K, 7 T, (c) 65 K, 1 T, and (d) 65 K 9 T for $B//c$. The same symbols are used in (a)–(d). A single function of B_{Φ} (unlike for T_{irr}/T_c) cannot explain the behavior of J_c .

Although T_c was not significantly different in the films presented in this manuscript, T_c enhancement is effective in improving J_c , and therefore, the effect of T_c should also be discussed. T_{irr} is a function of both T_c and B_{Φ} because: $T_{irr} = T_c \times T_{irr}/T_c = T_{irr}(T_c, T_{irr}/T_c(B_{\Phi})) = T_{irr}(T_c, B_{\Phi})$. $B_{irr} = 15$ T at 77 K in $\text{SmBa}_2\text{Cu}_3\text{O}_7 + \text{BHO}$ with B_{Φ} of ~ 1 T owing to the large T_c of 92.3 K;²⁰ but $B_{irr} = 8.6$ T at 77 K in our YBCO + BSO(2.7) sample with a T_c of 89.2 K and B_{Φ} of ~ 1.5 T—the difference in B_{irr} between the two samples originates from their differing T_c values. As shown in the inset of Fig. 4(a), $J_c/J_c(0T)$ for $B > B_{\Phi}$ was larger for the $\text{SmBa}_2\text{Cu}_3\text{O}_7 + \text{BHO}$ sample than for our YBCO + BSO(2.7) sample, owing to the $\text{SmBa}_2\text{Cu}_3\text{O}_7 + \text{BHO}$ sample's larger B_{irr} or, to be more precise, owing to the effect of the T_c term in T_{irr} (B_{irr}). This indicates that enhancing T_c improves $J_c/J_c(0T)$ for $B > B_{\Phi}$.

In summary, the microstructure, T_{irr} , and J_c – B curves of YBCO + BZO, YBCO + BSO, and YBCO + BHO films were analyzed. B_{Φ} of the films ranged from 1.5 T to 5 T, and the films exhibited ideal nanorod pinning. Regardless of BMO selection and vol. % content, T_{irr}/T_c curves depended only on B_{Φ} , while $J_c/J_c(0T)$ – B and F_p – B curves varied systematically with B_{Φ} : with increasing B_{Φ} , $J_c/J_c(0T)$ decreased at low magnetic field strengths, but increased at high magnetic field strengths. B_{Φ} determined T_{irr}/T_c or $J_c/J_c(0T)$, while the T_c term in T_{irr} and $J_c(0T)$ also had an effect on J_c .

This work was supported by Fundamental Research Developing Association for Shipbuilding and Offshore

(REDAS), The Japan Prize Foundation, and KAKENHI, Grant-in-Aid for Science Research (S), Grant No. 23226014.

- ¹J. L. Macmanus-Driscoll, S. R. Foltyn, Q. X. Jia, H. Wang, A. Serquis, L. Civale, B. Maiorov, M. E. Hawley, M. P. Maley, and D. E. Peterson, *Nat. Mater.* **3**, 439 (2004).
- ²P. Mele, K. Matsumoto, T. Horide, A. Ichinose, M. Mukaida, Y. Yoshida, S. Horii, and R. Kita, *Supercond. Sci. Technol.* **21**, 032002 (2008).
- ³H. Tobita, K. Notoh, K. Higashikawa, M. Inoue, T. Kiss, T. Kato, T. Hirayama, M. Yoshizumi, T. Izumi, and Y. Shiohara, *Supercond. Sci. Technol.* **25**, 062002 (2012).
- ⁴A. Xu, L. Delgado, N. Khatri, Y. Liu, V. Selvamanickam, D. Abraimov, J. Jaroszynski, F. Kametani, and D. C. Larbalestier, *APL Mater.* **2**, 046111 (2014).
- ⁵T. Horide, K. Matsumoto, P. Mele, A. Ichinose, R. Kita, M. Mukaida, Y. Yoshida, and S. Horii, *Appl. Phys. Lett.* **92**, 182511 (2008).
- ⁶A. Kiessling, J. Hanisch, T. Thersleff, E. Reich, M. Weigand, R. Huhne, M. Sparring, B. Holzapfel, J. H. Durrell, and L. Schultz, *Supercond. Sci. Technol.* **24**, 055018 (2011).
- ⁷T. Horide, T. Kawamura, K. Matsumoto, A. Ichinose, M. Yoshizumi, T. Izumi, and Y. Shiohara, *Supercond. Sci. Technol.* **26**, 075019 (2013).
- ⁸B. Maiorov, S. A. Baily, H. Zhou, O. Ugurlu, J. A. Kennison, P. C. Dowden, T. G. Holesinger, S. R. Foltyn, and L. Civale, *Nat. Mater.* **8**, 398 (2009).
- ⁹T. Horide, T. Kitamura, A. Ichinose, and K. Mastumoto, *Jpn. J. Appl. Phys., Part 1* **53**, 083101 (2014).
- ¹⁰C. Cantoni, Y. Gao, S. H. Wee, E. D. Specht, J. Gazquez, J. Meng, S. J. Pennycook, and A. Goyal, *ACS Nano* **5**, 4783 (2011).
- ¹¹A. Llordes, A. Palau, J. Gazquez, M. Coll, R. Vlad, A. Pomar, J. Arbiol, R. Guzman, S. Ye, V. Rouco, F. Sandiumenge, S. Ricart, T. Puig, M. Varela, D. Chateigner, J. Vanacken, J. Gutierrez, V. Moshchalkov, G. Deutscher, C. Magen, and X. Obradors, *Nat. Mater.* **11**, 329 (2012).
- ¹²L. K. Elbaum, L. Civale, G. Blatter, A. D. Marwick, F. Holtzberg, and C. Field, *Phys. Rev. Lett.* **72**, 1914 (1994).
- ¹³A. Mazilu, H. Safar, M. P. Maley, J. Y. Coulter, L. N. Bulaevskii, and S. Foltyn, *Phys. Rev. B* **58**, R8909 (1998).
- ¹⁴R. J. Olsson, W. K. Kwok, L. M. Paulius, A. M. Petrean, D. J. Hofman, and G. W. Crabtree, *Phys. Rev. B* **65**, 104520 (2002).
- ¹⁵T. Horide, K. Matsumoto, A. Ichinose, M. Mukaida, Y. Yoshida, and S. Horii, *Supercond. Sci. Technol.* **20**, 303 (2007).
- ¹⁶T. Horide, K. Matsumoto, P. Mele, Y. Yoshida, R. Kita, S. Horii, and M. Mukaida, *Phys. Rev. B* **79**, 092504 (2009).
- ¹⁷P. Mele, K. Matsumoto, A. Ichinose, M. Mukaida, Y. Yoshida, S. Horii, and R. Kita, *Supercond. Sci. Technol.* **21**, 125017 (2008).
- ¹⁸S. H. Wee, Y. L. Zuev, C. Cantoni, and A. Goyal, *Sci. Rep.* **3**, 2310 (2013).
- ¹⁹L. Radzihovsky, *Phys. Rev. Lett.* **74**, 4923 (1995).
- ²⁰A. Tsuruta, Y. Yoshida, Y. Ichino, A. Ichinose, K. Matsumoto, and S. Awaji, *Supercond. Sci. Technol.* **27**, 065001 (2014).
- ²¹S. Awaji, Y. Yoshida, T. Suzuki, K. Watanabe, K. Hikawa, Y. Ichino, and T. Izumi, *Appl. Phys. Express* **8**, 023101 (2015).
- ²²T. Horide, K. Matsumoto, K. Osamura, A. Ichinose, M. Mukaida, Y. Yoshida, and S. Horii, *Phys. C* **412–414**, 1291 (2004).
- ²³V. Selvamanickam, M. H. Gharahcheshmeh, A. Xu, E. Galstyan, L. Delgado, and C. Cantoni, *Appl. Phys. Lett.* **106**, 032601 (2015).
- ²⁴H. Kupfer, T. Wolf, C. Lessing, A. A. Zhukov, X. Lancon, R. Meier-Hirmer, W. Schauer, and H. Wuhl, *Phys. Rev. B* **58**, 2886 (1998).
- ²⁵D. R. Nelson and V. M. Vinokur, *Phys. Rev. B* **48**, 13060 (1993).
- ²⁶B. Dam, J. M. Huijbregtse, F. C. Klaassen, R. C. van der Geest, G. Doornbos, J. H. Rector, A. M. Testa, S. Freisem, J. C. Martinez, B. Stauble-Pumpin, and G. Griessen, *Nature* **399**, 439 (1999).